RSC Advances

PAPER

View Article Online
View Journal | View Issue

Cite this: *RSC Adv.*, 2015, **5**, 89879

Cetyl alcohol mediated fabrication of forest of Ag/Mn_3O_4 nanowhiskers catalyst for the selective oxidation of styrene with molecular oxygen†

Shankha S. Acharyya, Shilpi Ghosh, Sachin K. Sharma and Rajaram Bal*

Received 31st August 2015
Accepted 8th October 2015

DOI: 10.1039/c5ra17630a

www.rsc.org/advances

Cetyl alcohol-mediated water-based preparation of nanocrystalline Ag/Mn_3O_4 catalyst has been reported in a one-pot preparation method. This catalyst has been characterized by XRD, XPS, SEM, TEM, STEM-mapping, FTIR, Raman and ICP-AES. Electron microscopy displayed the formation of whisker-like one-dimensional structure. TEM-images revealed the formation of ultrasmall Ag (with average size 5 nm), anchored on hausmannite-type tetragonal Mn_3O_4 spinel (with diameter 30–40 nm). It was found that the catalyst can effectively oxidize styrene with molecular O_2 as oxidant. The effect of different reaction parameters like reaction temperature, pressure of oxygen gas, reaction time *etc.* have been investigated in detail. A styrene conversion of 67% with a styrene-oxide selectivity of 100% accomplished over this catalyst. Nano-whiskers like unique morphology of the catalyst and the thorough dispersion of Ag nanoparticles on Mn_3O_4 spinel support are the detrimental factors of the reactivity of the catalyst. The catalyst did not show any leaching up to five reuses, showing its true heterogeneity nature.

Introduction

Direct functionalization of hydrocarbons to form oxygenated products under mild conditions by means of catalytic oxidation of C–H bonds is a major challenge, since this path provides as the key to the formation of value-added oxygenated chemicals and pharmaceuticals.[1] Among many oxidation reactions, catalytic oxidation of styrene is one of the most important instances since the reaction gives valuable oxygenated compounds like styrene oxide which can serve as precursors for many chemical products like perfumes and drugs *etc.*[2] Industrially, oxidation of styrene is carried out by using stoichiometric amounts of organic peracids as oxidant.[3] But production of a specific oxygenate selectively, with high yield is a great challenge to the researchers; so, many researchers came forward to sort out the problem using various oxidants like TBHP,[4] H_2O_2,[5] molecular oxygen,[6] and a mixture of TBHP and molecular oxygen.[7]

In the light of green chemistry, metal-catalyzed aerobic oxidation represents the most elegant and environmentally friendly route for a large-scale production of invaluable oxidation products.[8] The utilization of molecular oxygen for a catalytic oxidation without reducing reagents or radical initiators is a goal in the field of catalysis. This is due to the highest content of active oxygen in molecular oxygen compared to other oxidants. However, only a few homogeneous epoxidations of olefins with molecular oxygen at 1 atm without reducing agents/radical initiators have been developed to resolve difficulty with either persuasion of the catalysts to act as a stoichiometric oxidant or degradation of their organic ligands.[9] Moreover, the poor product selectivity obtained in aerobic processes is one of the major drawback for using molecular oxygen as the terminal oxidant for the formation of epoxides.[10] Additionally, the limited number of catalysts available for direct activation of molecular oxygen, effectively restricts its use. Thus, selective catalytic epoxidation methods with molecular oxygen are highly desirable. Many researchers, in this regard, came forward to produce SO from styrene using molecular O_2 with high yield. Rezaeifard *et al.* reported preparation of keplerate polyoxomolybdate nanoball {Mo132}, that afforded a SO yield of 93% at 25 °C under 1 atm O_2.[10] Wang *et al.* reported positively charged bulk Au particles with size of 20–150 nm, which afforded a styrene conversion of 27%, with a SO selectivity of 30% using 1.5 bar pressure (O_2), and 100 °C.[11] Very recently, Li and his group reported preparation of ultrathin copper oxide (CuO) nanorods with diameters of ~3.6 nm, over which a styrene conversion of 96%, with a selectivity to SO of 81% was achieved.[12]

However, to accomplish a process in nontoxic solvents, particularly in aqueous media to get satisfactory yield of SO is really a challenge in terms of green chemistry.[13] Recently, reactions of water insoluble organic compounds that take place in aqueous suspensions have received a potential attention because of their high efficiency and straightforward synthetic protocols.[14] Nevertheless, such reactions are still rare and lack generality. Therefore, a true heterogeneous catalyst (devoid of

Catalytic Conversion & Processes Division, CSIR-Indian Institute of Petroleum, Dehradun-248005, India. E-mail: raja@iip.res.in

† Electronic supplementary information (ESI) available: SEM and TEM images, SEM-EDAX images *etc.* See DOI: 10.1039/c5ra17630a

leaching properties) with high selective nature is highly demanding in the field of catalysis.

The heterogeneous epoxidation of olefins by silver-based catalysts is an important process in chemical technologies,[15] and the catalytic properties of AgNPs in oxidation reactions strongly depend on the particles' size and stability and the nature of the support.

Recently, study on morphology-dependent catalytic activity has attracted considerable interest in heterogeneous catalysis.[16] The design of catalytically active nanomaterials with specific and tunable morphology to achieve remarkable catalytic performance by exposing their crystal facets is of great significance. One-dimensional (1D) nanomaterials (such as wires, rods, tubes, belts *etc.*), which have been emerging under said area, are drawing growing attention for the specific physical properties that they display compared to their bulk counterparts.[17] Therefore, 1D nanomaterials have been the focus of extensive research in recent years, owing to their potential applications.[18] For a surface-related application such as heterogeneous catalysis, a key advantage of nanomaterials is provided by the increased surface-to-volume ratio that accompanies the decrease in the size of the catalyst particles. Ag–Mn-bimetallic oxide nanostructures have been a topic of potential interest due its efficacy in super capacitance,[19] low-temperature CO oxidation,[20] catalytic oxidation of benzene,[21] toluene,[22] alcohols,[23] *etc.* In recent years, our group reported the facile preparation of various bimetallic-1D nanomaterials;[8b,24] our group also reported that cetyl alcohol is a long-tailed alcohol (C-16) and can be used as a surfactant that promotes the formation of nanoparticles.[25] Being inspired by our previous reports, we came forward to synthesize 1D Ag–Mn oxide nanostructures in a facile water-based method at room temperature, mediated by cetyl alcohol. Here in this paper, we report cetyl alcohol (CtOH)-mediated preparation of one-dimensional (1D) Ag/Mn_3O_4 nanowhiskers catalyst (where supported Ag nanoparticles are 2–5 nm in size). The catalyst was proved to be highly effective in epoxidation of styrene to SO in water medium, by means of aerial oxidation. A styrene conversion of 67% and a SO selectivity of 100% were accomplished over this catalyst. To the best of our knowledge, there is no literature that reports the preparation of one-dimensional (1D) Ag/Mn_3O_4 nanowhiskers catalyst, mediated by CtOH, that affords such a high yield of SO from styrene using molecular O_2 as oxidant.

Experimental

Materials

Anhydrous manganese(II) chloride ($MnCl_2$), anhydrous silver nitrate ($AgNO_3$), cetyl alcohol, hydrazine (80% aq. solution), ammonium hydroxide, styrene (purity > 99.9%), deionized water (HPLC grade) were purchased from Sigma-Aldrich Co. All the chemicals were used without further purification.

Methods

The Ag/Mn_3O_4 nanowhiskers catalyst was synthesized by modifying our own preparation method.[24] In a typical preparation method, 11 g anhydrous manganese chloride was dissolved in 24 g water to give a pink-coloured solution. Then, aqueous solution of 0.74 g anhydrous silver nitrite was added dropwise. The pH of solutions was measured by pH meter, which was standardized for pH measurement prior to use. By gradual addition of few drop ammonia solution, the pH of the solution was made 8; the colour of the solution became greyish gradually. Then aqueous (hot) solution of cetyl alcohol 1.06 g was added in the mixture, followed by intensive stirring for 2 h. A solution of 0.3 hydrazine monohydrate (80% aqueous solution) was added drop wise to the well stirred mixture at RT by simultaneous, vigorous agitation. All the reagents were used maintaining the ratio: $Ag : CtOH : hydrazine : H_2O = 1 : 1 : 1 : 300$. The mixture was stirred vigorously for 30 min. After 30 min stirring, the mixture was aged at 40 °C for overnight (12 h). After that, the mixture was agitated thoroughly by ethanol. Thick greyish precipitation occurred. After that, these white fluffy solid products (precipitates) were collected by centrifugation at 7500 rpm and washed with water and ethanol several times prior to drying in air at 100 °C for 6 h. The resulting dry powder was transferred to a quartz reactor inside a tubular resistance furnace for calcination at 500 °C in argon atmosphere. After calcinations, the so obtained deep black-coloured powder was collected for characterization and reactions.

Characterization techniques

X-ray power diffraction (XRD): powder X-ray diffraction patterns were collected on a Bruker D8 advance X-ray diffractometer fitted with a Lynx eye high-speed strip detector and a Cu K_α radiation source using Cu Kα radiation with a wavelength of 1.5418 Å. Diffraction patterns in the 2–80° region were recorded at a rate of 0.5 degrees (2θ) per minute. The resulting XRD profiles were analyzed to identify the crystal phase of the compound using reference standards. The line width of the most intense XRD peak was taken for estimation of crystallite size by the Scherrer equation. Scanning electron microscopy (SEM): scanning electron microscopy images were taken on a FEI Quanta 200 F, using tungsten filament doped with lanthanum hexaboride (LaB_6) as an X-ray source, fitted with an ETD detector with high vacuum mode using secondary electrons and an acceleration tension of 10 or 30 kV. Samples were analyzed by spreading them on a carbon tape. Energy dispersive X-ray spectroscopy (EDX) was used in connection with SEM for the elemental analysis. The elemental mapping was also collected with the same spectrophotometer. Samples were subjected to scanning electron microscope analysis to understand the shape, size, and morphology properties. Transmission electron microscopy (TEM): the particle size and distribution of the samples were analyzed by TEM, JEOL JEM 2100 microscope, and samples were prepared by mounting an ethanol-dispersed sample on a lacey carbon Formvar coated Cu grid. X-ray photoelectron spectroscopy (XPS): X-ray photoelectron spectra were recorded on a Thermo Scientific K-Alpha X-ray photoelectron spectrometer and binding energies (±0.1 eV) were determined. The resulting spectra were analyzed to

identify the different oxidation states of the silver and manganese ions present in the sample. Prior to the analysis, the spectra were calibrated with reference to C 1s observed at a binding energy of 284.5 eV. Inductively coupled atomic absorption spectroscopy (ICP-AES): chemical analyses of the metallic constituents were carried out by Inductively Coupled Plasma Atomic Emission Spectrometer; model: PS 3000 UV, (DRE), Leeman Labs, Inc, (USA). Raman spectra was measured at 298 K by using a Laser Raman Spectrometer (JASCO, NRS-3100) with the 532 nm line from a diode-pumped solid-state laser for excitation. Fourier transform infra-red (FT-IR) spectra were recorded on a Thermo Nicolet 8700 (USA) instrument with the operating conditions: resolution: 4 cm^{-1}, scan: 36, operating temperature: 23–25 °C and the frequency range: 4000–400 cm^{-1}. Spectra in the lattice vibrations range were recorded for wafers of sample mixed with KBr.

Oxidation of styrene

Catalytic reactions were carried out in a 100 mL PTFE lined, stainless-steel, high-pressure batch reactor. The reactor was charged with styrene (1 g), water as dispersing media (5 mL), *tert*-butanol (0.50 g) as an internal standard and catalyst (0.2 g). The reactor was pressurised with oxygen gas, stirred and heated. Small aliquots of the reaction mixture were taken carefully periodically for GC analysis. At the end of the reaction, the solid particles (catalyst) were separated by filtration and the products were analysed by Gas Chromatograph (GC, Agilent 7890) connected with a HP5 capillary column (30 m length, 0.28 mm id, 0.25 μm film thickness) and flame ionisation detector (FID). Chem Station software was used to collect and analyze the respective GC-data. The relative error of product determination did not exceed ±5%. The styrene conversion and SO formation were calculated using a calibration curve (obtained by manual injecting the authentic standard compounds). The individual yields were calculated and normalized with respect to the GC response factors. The product identification was carried out by injecting the authentic standard samples in GC and GC-MS.

For the reusability test, the catalyst was repeatedly washed with acetonitrile and acetone and dried overnight at 110 °C and used as such, without regeneration. In order to check the metal leaching the mother liquor was then analyzed using ICP-AES.

Material balance

We have performed the C-balance for the most of the experiments and have also done the material balance for few experiments. The estimated error in analysis arising due to sampling and handling losses was ±5.

Results and discussion

Catalyst characterization

The X-ray-diffraction (XRD) pattern was carried out to investigate the crystal structure and phase purity of the catalyst. XRD (Fig. 1) of the Ag–Mn catalyst showed the peaks at $2\theta = 28.8°$, 36.08°, 44.4°, 59.8°, 69.6° *etc.* which can be indexed to hausmannite-type tetragonal Mn_3O_4 with specific group $I4_1/amd$ [JCPDS 24-0734], with a maximum intensity at 36.085°; apart from these, two small peaks at 44.4° and 64.6° were noticed in the diffractogram (Fig. 1). These two peaks can be attributed to the presence of (200) and (220) planes of metallic silver as confirmed from [JCPDS 04-0783]. However, no other peak due to impurities can be observed in the diffractogram which unveiled the highly phase-purity of the product. The XRD pattern of the spent catalyst was indicate that the catalyst remains unchanged even after 5 reuses. X-ray photoelectron spectroscopy (XPS) analyses confirmed the presence of metallic silver in the fresh sample from the corresponding Ag $3d_{5/2}$ and Ag $3d_{3/2}$ binding energy values of 368.2 eV and 374.2 eV respectively (Fig. 2).[26] The XPS spectra of Mn in the sample (Fig. 3) showed that, Mn $2p_{3/2}$ peak appeared at 641.5 eV and that of Mn $2p_{1/2}$ peak at 653.3 eV, indicating that the element Mn is in the state of Mn^{2+}.[27] The spin–orbit splitting is the difference between the binding energy values of Mn $2p_{3/2}$ and Mn $2p_{1/2}$ levels. Observed spin–orbit splitting is 11.8 eV. These

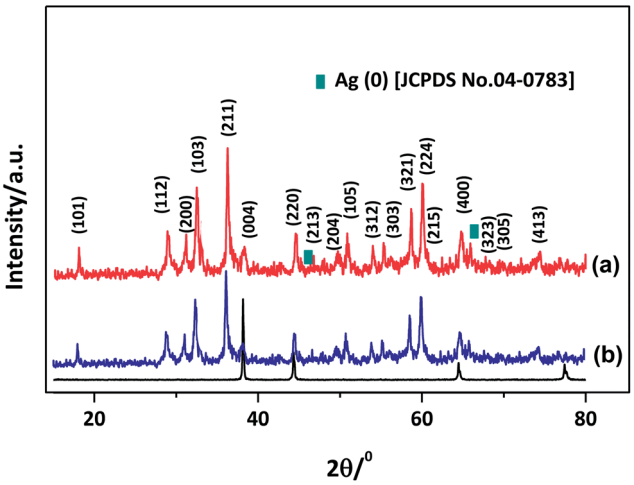

Fig. 1 XRD diffractogram of (a) fresh and (b) spent Ag/Mn_3O_4 nano-whiskers catalyst (after 5 recycles) and that of (c) commercial Ag.

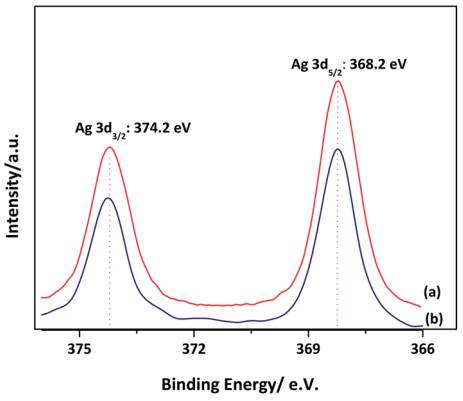

Fig. 2 Ag 3d core-level spectra (XPS) of (a) fresh and (b) spent Ag/Mn_3O_4 nano-whiskers catalyst.

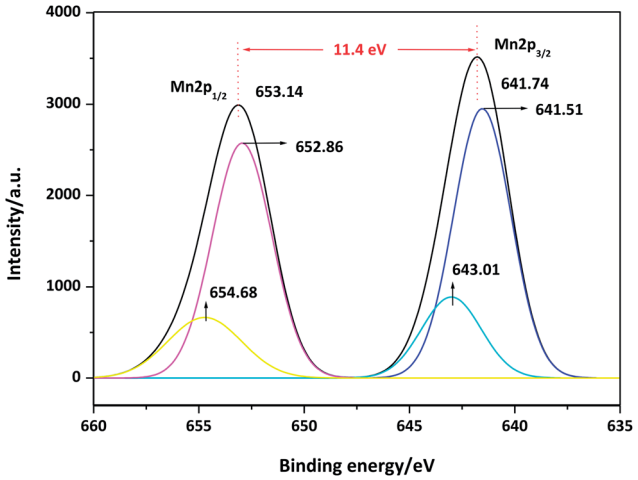

Fig. 3 Mn 2p core-level spectra (XPS) of fresh Ag/Mn_3O_4 nano-whiskers catalyst.

results are in accordance with the reported data of Mn $2p_{3/2}$ and Mn $2p_{1/2}$ in Mn_3O_4. The corresponding Ag 3d binding energy of the spent catalyst ~368.3 eV, confirms that the oxidation state of metallic silver does not change during catalysis. To further investigate the surface property and to detect subtle phase information of the composite, we conducted Raman (Fig. 4) and FTIR-spectrum (Fig. 7) analyses of the sample. Four major peaks were observed in the Raman spectrum. The strongest peak at 659 cm^{-1} and three peaks at 291 cm^{-1}, 321 cm^{-1}, and 374 cm^{-1} in the Raman spectrum are the indicative of Mn_3O_4 in the sample[28] and exclude the presence of any other oxide of Mn. Moreover, the nature of the peaks in the Raman spectrum of the spent catalyst was almost same as that of the fresh catalyst, reflecting the high structural stability of the catalyst under the reaction condition. The shape and morphology of the product have been investigated using the SEM (Fig. 5). SEM image revealed that the sample possesses several thousands of throughout uniform nano-rods and is devoid of serious aggregation. Each rod with a length of *ca.* ~5.5 μm was visualized from SEM image. The corresponding SEM-EDAX image (Fig. 5b) further confirmed the presence of Ag, Mn and O in the sample and no sort of impurity

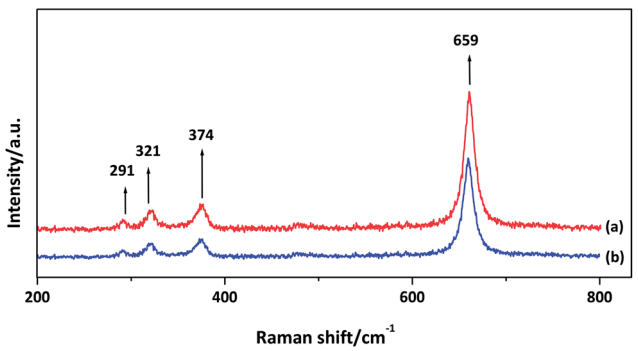

Fig. 4 Raman spectra of (a) fresh and (b) spent Ag/Mn_3O_4 nano-whiskers catalyst.

like C or Cl (which are visualized in the SEM-EDAX image of the uncalcined catalyst, Fig. S1, ESI†), which demonstrated the complete removal of the surfactant upon calcinations. This fact was further proved from the FTIR analyses of the uncalcined catalyst (Fig. 8). The TEM image in Fig. 6a–f illustrates the network structure due to the assembly of finely grown flexible Ag–Mn nano-whiskers. The magnified view in Fig. 6c and d reveal that the rods are usually 30–40 nm in diameter. In addition, the SAED (selected area electron diffraction) pattern (Fig. S2, ESI†) also displayed a polycrystalline nature of the rod-like structure, indicating that the Ag–Mn nanorods are randomly orientated. TEM images with comparative higher resolutions (Fig. 6c and d) revealed that the catalyst is composed of highly dispersed very small silver nanoparticles of ~2–5 nm on Mn_3O_4 support. The interplanar spacing of the lattice fringe distance of 0.28 nm indicates the [103] lattice spacing of Mn_3O_4 (ref. 29) which was clearly discriminated from of 0.23 nm corresponds to [111] plane of Ag (Fig. 6e).[24] The corresponding TEM histogram of Ag nanoparticles showed a very narrow particle size distribution with sizes between 2.5 and 6.5 nm (Fig. 6c, inset). Furthermore, the TEM image (Fig. 6f) of the spent catalyst showed that the topology and the silver particle size (and its size distribution, Fig. 6b) of the catalyst were hardly changed after five reuses. This assignment is tentative and requires further confirmation by FTIR measurements, since FTIR spectra of the materials are conducted to verify the integrity of the structure of the examined materials (Fig. 7). Some bands were detected at 2800–3020 cm^{-1}, which can be attributed to the CTA-moiety. The FTIR spectrum of CtOH shows two intense bands at 2918 and 2846 cm^{-1}, corresponding to the asymmetric and symmetric stretching vibrations of C–CH in the methylene chains. The sharp bands at 1450–1500 cm^{-1} were specified as the deformation of $–CH_2–$ and –CH, and the weak band at 3011 cm^{-1} as the $C–CH_3$ asymmetric stretching vibrations of the solid surfactant.[30] The frequencies above 1600 cm^{-1} to 3000 cm^{-1} (Fig. 7c) are due to CH_2 symmetric and antisymmetric vibrations, respectively.[30] It can be inferred that, the mutual interactions between CtOH and the Ag–Mn surface have taken place. However, these typical frequencies were absent when the material was calcined at 500 °C (fresh catalyst) in the case of the prepared catalyst, which indicated that, the embedded CtOH moieties have been completely removed from the catalyst (uncalcined) surface during calcination. Thus, no sort of template remains on the catalyst (calcined) surface and therefore frequencies due to the template (cetyl alcohol) completely disappear after calcination (Fig. 7a). After calcination, some new bands were visible in the FTIR-spectra of the catalyst (Fig. 7a). The regions from 750–600 cm^{-1} and 600–450 cm^{-1} correspond to the Mn–O stretching and bending vibrations. The absorption of the Mn–O lattice vibrations around 724 and 525 cm^{-1} in the spectrum is indicative of a tetragonally distorted cubic lattice. These absorption peaks may be associated with the coupling mode between Mn–O stretching modes of tetrahedral and octahedral sites.[31] The band at 612 cm^{-1} in the spectrum of the catalyst was assigned to Mn–O vibrations of bivalent manganese ions in tetrahedral co-

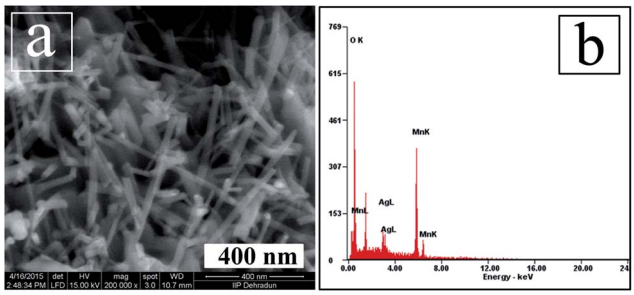

Fig. 5 (a) SEM and (b) SEM-EDAX diagram of Ag/Mn_3O_4 nano-whiskers catalyst.

ordination.[31] Moreover, it was also confirmed from the FTIR diagram that, there was no structural deformation in the catalyst even after 5 recycles (Fig. 7b).

Although the morphological and crystalline characteristics of Ag–Mn nanorods can be identified from 2D TEM images, some important information on the material may still be difficult to detect due to the limitation of 2D projection in the TEM technique. Therefore the sample was undergone STEM-elemental mapping analyses (Fig. 8), which displayed the thorough dispersion of metallic Ag-NPs on the Mn_3O_4-rods (support).[32]

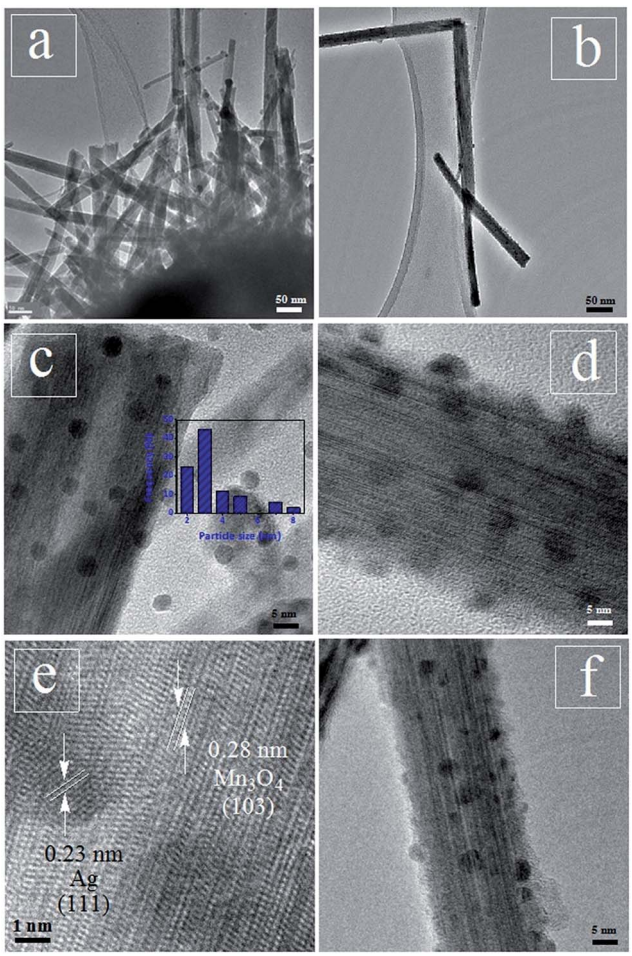

Fig. 6 TEM image of (a–e) the fresh catalyst at ascending magnifications and (f) that of spent Ag/Mn_3O_4 nano-whiskers catalyst.

Generation of one-dimensional (1D) nanowhiskers

The evolution of whiskers like structure is really interesting although the mechanism is not very clear. Cetyl alcohol, synthesis-stirring time *etc.* play important role in determining the morphology of the final nanostructures. As per LaMer plot[33] for the crystallization nucleation growth process and Tran's point, the nucleation rate increases with decreasing surface energy. The surfactant can affect surface energy and thus control the nucleation rate. According to Gibbs–Wulff theory, the equilibrium shape of a crystal is one that minimizes the surface energy for a given enclosed volume. If the surface energy is isotropic, the equilibrium shape will be spherical as the sphere has the minimum surface area. Inorganic nanoparticles often lead to spherical particles as this represents the lowest possible surface energy. 1D nanostructures is generated, if the surface energy is anisotropic.[33]

To explore the formation mechanism of Ag–Mn nanowhiskers, a series of time-dependent experiments were performed. In the absence of CtOH, agglomerated particles with indefinite shapes and larger sizes were obtained (Scheme 1A, Fig. S3a, ESI†). However, when the mixture was kept for 3 h aging, followed by calcinations, the product so obtained displayed that numerous nanoparticles assembled together and in a definite direction, the growth of the assembly occurred (Scheme 1B, Fig. S3B, ESI†) 12 h aging time was proved to be optimum condition for the growth of the whiskers-type morphology. The TEM image of the sample displayed that almost homogeneously formed nanorods (1D) with diameter ~50 nm grew in a definite direction and displayed whiskers-like morphology (Scheme 1E). While the aging time was prolonged to 24 h, these nanorods fused together by means of Ostwald ripening process and produced larger, indefinite-shaped aggregates (Scheme 1D, Fig. S3d, ESI†).

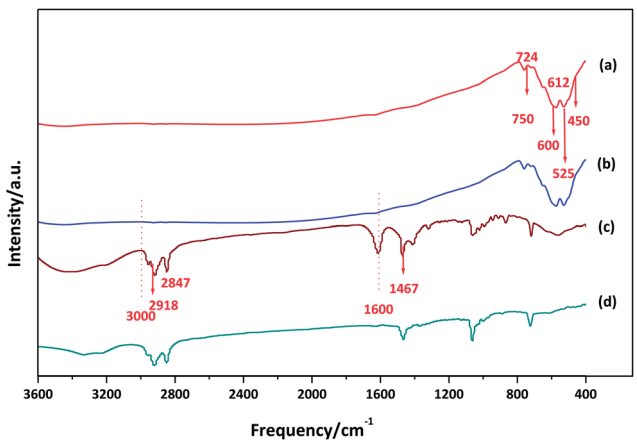

Fig. 7 FTIR diagram of (a) cetyl alcohol, (b) uncalcined, (c) fresh and (d) spent Ag/Mn_3O_4 nano-whiskers catalyst.

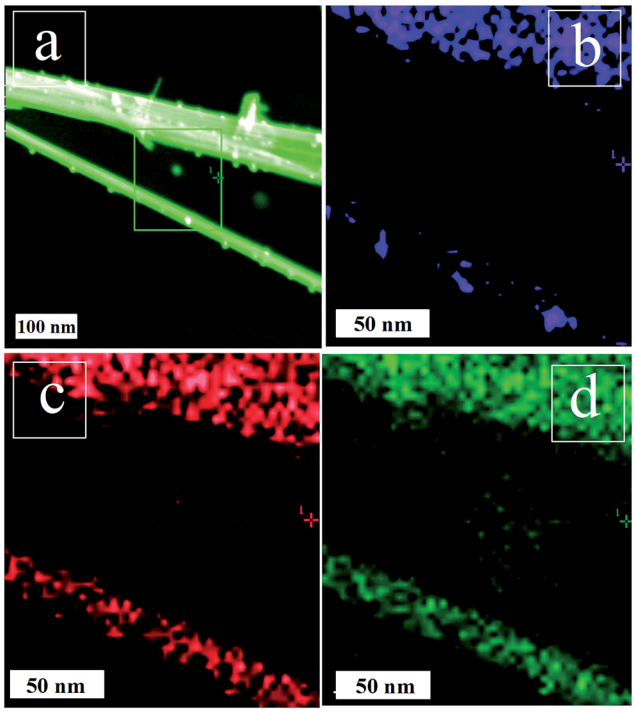

Fig. 8 (a) STEM image and STEM-elemental mapping of (b) Ag, (c) Mn and (d) O in the Ag/Mn_3O_4 nano-whiskers catalyst.

As a cationic surfactant, CtOH is an ionic compound that ionized completely in water: quantities of anions OH^-, $[MnO_x]^{n-}$ and Ag and cations CTA^+, Ag^+ existed in basic solution.[24] Therefore, cooperative self-assembly between ionic CtOH molecules and charged species is built *via* electrostatic interaction in reaction solution. The formation of nearly spherical aggregates of nanoparticles after 12 h aging time may be brought from the strong electrostatic attraction between positive CTA^+ cations and negative OH^- anions on the surface of nanoparticles as well as the hydrophobic interactions and van der Waals attraction caused by adjacent CtOH adsorbing on Ag–Mn nanoparticles. All these factors contribute greatly for the generation of whiskers-like morphology of the sample. Therefore, we tentatively, suggest that, CtOH-micelles in the solution and even aging time directly take part in the shape-controlled synthesis of Ag/Mn_3O_4 nanowhiskers catalyst.

Catalytic activity of Ag/Mn_3O_4 nanowhiskers in aerial oxidation of styrene

The Ag/Mn_3O_4 nanowhiskers catalyst was proved to be highly efficient in oxidation of styrene to styrene oxide with molecular O_2 as oxidant. Table 1 shows the activities of Ag/Mn_3O_4 nanowhiskers catalyst in the aerial oxidation of styrene to styrene oxide and the comparative studies of other parent oxides (commercial) catalysts at 80 °C reaction temperature and 10 bar pressure (O_2). Blank test (without any catalyst) was performed (entry 1, Table 1), where no conversion of styrene was observed, reflecting the necessity of the catalyst. When Ag/Mn_3O_4 nanowhiskers was introduced as catalyst, it afforded a styrene conversion of 67%, with selectivity to styrene oxide was 100%; that means solely one product was detected. However, commercial Ag_2O, Mn_3O_4, and even metallic Ag catalyst did not show any activity (entry 2–4, Table 1). Conventional catalyst prepared by impregnation method also showed negligible activity (Ag_2O–$Mn_3O_4^{IMP}$ entry 5, Table 1). It was observed from Table 1 that this catalyst (Ag_2O–$Mn_3O_4^{IMP}$) showed 13 times lesser activity than our so prepared catalyst in terms of TON (turn over number). The reason can be attributed to the comparatively smaller size of Ag (supported) nanoparticles catalyst possess comparatively high specific surface area which corresponds to higher dispersion of the catalyst that leads to the availability of more exposed surface active sites, where the catalytic reaction takes place. The poor catalytic activity of the impregnated catalyst may be attributed to their irregular shape and larger particles size (as confirmed from its SEM image, Fig. S4, ESI†) which limits the accessibility of the catalyst towards the reacting substrates.

The reaction activities and product selectivity strongly depend on the reaction parameters of temperature and O_2 pressure in the aqueous reaction solutions. At room temperature, the conversion of styrene was too poor to be detected. Upon increasing the temperature, the styrene conversion was increased (Fig. 9). The maximum selectivity to SO be obtained at 80 °C. Above this reaction temperature, although greater conversion of styrene was observed, but the selectivity to SO was noticed to be lesser due to the formation of benzaldehyde. Similarly, the effect of reaction pressure in the range of 5–15 bar was investigated and the corresponding results are depicted in Fig. 10. At atmospheric pressure, we conducted the reaction (at 80 °C), but, we observed very very poor conversion of styrene (~1%). With increased pressure of O_2, we observed that, upto 10 bar pressure, both the conversion of styrene and selectivity to SO increase monotonically. But, after 10 bar pressure, although conversion of styrene was noticed, but selectivity to SO started decreasing; this can attributed to the fact that, high pressure compelled to react styrene, beyond its optimization level. Maintaining all the optimum conditions, we carried out the reaction for hours. We noticed that, 25 h was required to get 67% yield of SO (Fig. 11). However, beyond this time, selectivity to SO was observed to be decreased; probably this occurred due to the fact that, with time, SO converted to benzaldehyde under said reaction conditions.

In contrast, our prepared catalyst possesses ultrasmall Ag, which is dispersed on Mn_3O_4 nanowhiskers in a thorough manner, which efficiently oxidize styrene to SO; probably, synergistic interaction between Ag and Mn_3O_4 nanowhiskers in the catalyst plays a vital role in this reaction. To prove this hypothesis, we took same type of catalyst, with Ag loading is 11.7% (where Ag nanoparticles are aggregated to form larger Ag-particles, as confirmed from TEM diagram Fig. S5, ESI†). We noticed that, further increment in content of Ag to 11.7%, the catalytic efficiency decreased (entry 8, Table 1). This may be attributed to the slightly aggregation of the Ag-NPs on the surface of Mn_3O_4 nanorods, resulting in the decrease of the number of active sites on the sample of the catalyst (Fig. S5, ESI†).

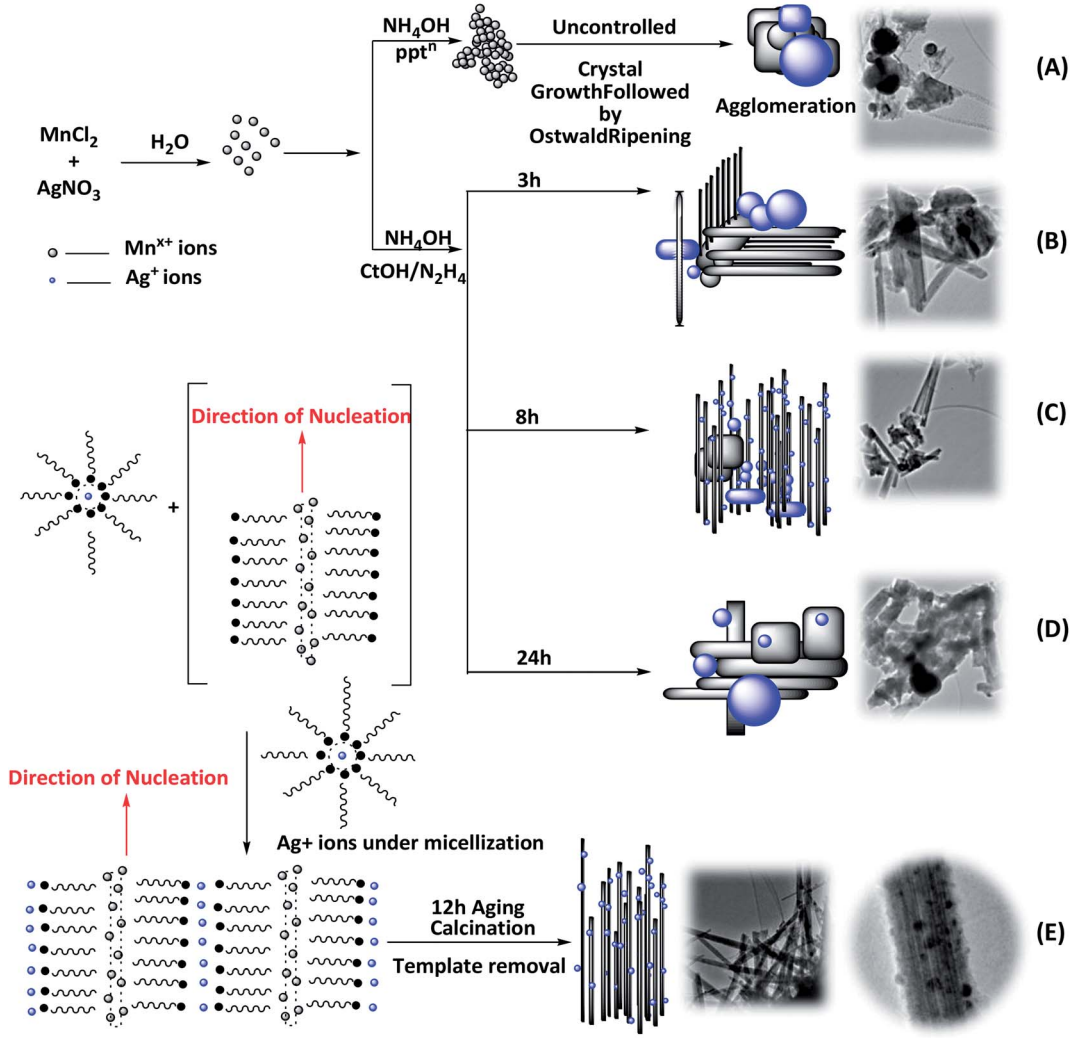

Scheme 1 Pictorial presentation of generation of Ag–Mn nanocomposites with various morphologies.

Table 1 Activities of the different catalysts for styrene oxidation[a]

Entry	Catalyst	C_S[b] (%)	S_{SO}[c] (%)	Y_P[d] (%)	TON[e]
1	No catalyst	—	—	—	—
2	Ag^{COM}	0.8	47	0.37	—
3	Ag_2O^{COM}	—	—	—	—
4	$Mn_3O_4^{COM}$	0.5	45	0.22	—
5	Ag_2O–$Mn_3O_4^{IMP}$	15.5	57	8.8	3.88
6[f]	$AgMn^{NR6.7}$	67	100	67	51.8
7[g]	$AgMn^{NR6.7}$	60	96	57.6	44.4
8[h]	$AgMn^{11.7}$	75	80	60	46.37

[a] Typical reaction conditions: solvent (H_2O) = 5 mL, substrate (styrene) = 1 g, catalyst = 0.2 g, pressure (O_2) = 10 bar; reaction temperature = 80 °C; time = 25 h. [b] C_S = conversion of styrene based upon the FID-GC using ^{t}BuOH as external standard = [moles of styrene reacted/initial moles of styrene used] × 100. [c] S_P = selectivity to SO = [moles of products produced/moles of cyclohexane reacted] × 100. [d] Y_P = yield of SO = $C_S \times S_{SO}/100$. [e] TON = turnover number calculated by moles of SO formed/one mole of Ag in the catalyst present as supported Ag(0). [f] Fresh. [g] Spent (after 5 recycles) Ag–Mn nanorods catalyst (Ag loading 6.7%). [h] Catalyst with Ag loading 11.7%.

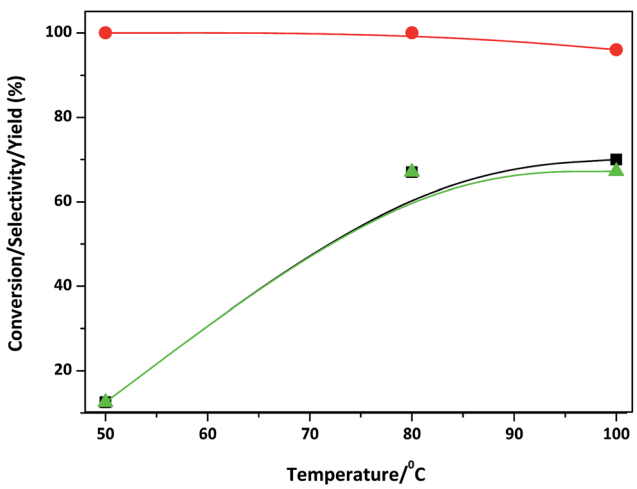

Fig. 9 Effect of temperature on styrene oxidation. [■] Conversion of styrene; [●] selectivity to SO; [▲] yield of SO. Reaction condition: styrene = 1 g; catalyst = 0.2 g; pressure (O_2) = 10 bar; time = 25 h.

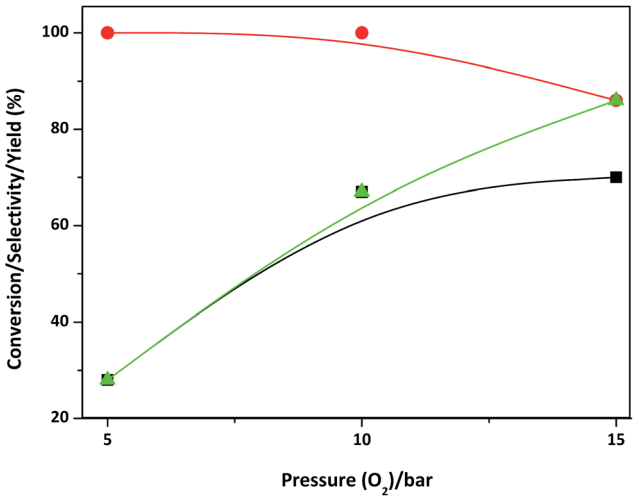

Fig. 10 Effect of pressure on styrene oxidation. [■] Conversion of styrene; [●] selectivity to SO; [▲] yield of SO. Reaction condition: styrene = 1 g; catalyst = 0.2 g; temperature = 80 °C; time = 25 h.

Reusability test

The efficiency of a heterogeneous catalyst is evaluated in terms of its recyclability and stability. The reusability of the Ag/Mn_3O_4 nanowhiskers catalyst was studied without any regeneration. After each run, the catalyst was filtered during hot condition and repeatedly washed with acetonitrile and acetone and dried overnight at 100 °C and used as such. We observed that the catalyst showed negligible change in its activity (entry 7, Table 1 & Fig. 12). The amount of Ag and Mn present in the catalyst after 5 reuse was almost same as the fresh catalyst (estimated by ICP-AES) confirming the true heterogeneity of the catalyst. After 5 recycles, negligible amount of leaching of Ag and Mn was detected by ICP-AES (concentration of both metals were <2 ppb).

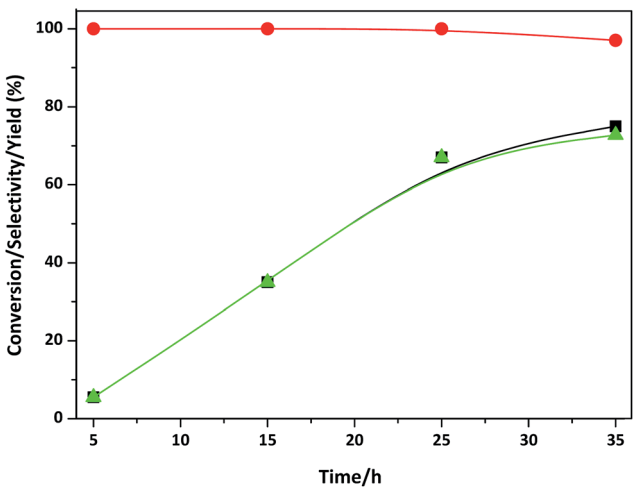

Fig. 11 Effect of time on styrene oxidation. [■] Conversion of styrene; [●] selectivity to SO; [▲] yield of SO. Reaction condition: styrene = 1 g; catalyst = 0.2 g; pressure (O_2) = 10 bar; temperature = 80 °C.

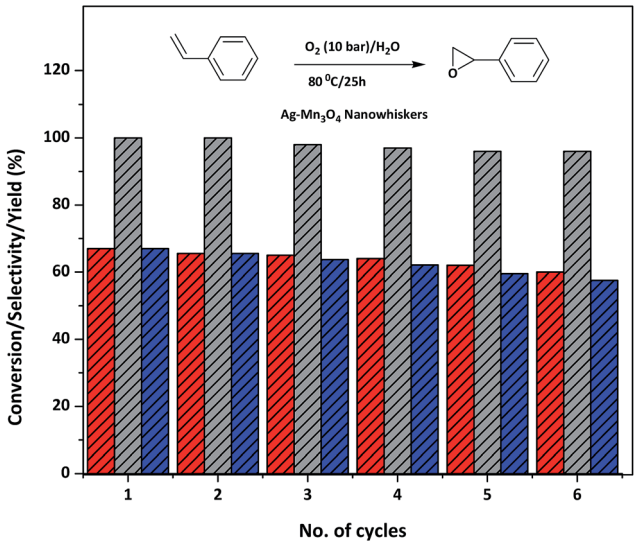

Fig. 12 Reusability test on catalytic aerobic oxidation of styrene to styrene oxide. [■] Conversion of styrene; [■] selectivity to SO; [■] yield of SO. Reaction condition: styrene = 1 g; catalyst = 0.2 g; pressure (O_2) = 10 bar; temperature = 80 °C; time = 25 h.

Conclusions

In summary, we have presented facile, water based, low temperature synthesis of ultrasmall Ag nanoparticles supported on Mn_3O_4 spinel with a unique one-dimensional nano-whiskers structure. The initial investigation showed that, it was a 2-stage process where nanoparticles were formed first, followed by organized assembly of these nanoparticles into nanorods. It was possible to tune the morphology of the Ag–Mn composites varying the preparation conditions. This synthesis could easily be scaled up due to its simplicity. Moreover the high thermal stability and reusability of the catalyst and its excellent ability in oxidation of styrene to styrene oxide using molecular O_2 as oxidant and may be a potential alternative path of the conventional process.

Acknowledgements

R. B. thanks CSIR, New Delhi, for financial support in the form of the 12 FYP Project (CSC-0125, CSC-0117). The Director, CSIR-IIP is acknowledged for his help and encouragement. The authors thank ASD Division, IIP for the analytical services.

Notes and references

1 (*a*) K. Kamata, K. Yonehara, Y. Nakagawa, K. Uehara and N. Mizuno, *Nat. Chem.*, 2010, **2**, 478–483; (*b*) C. Jia, T. Kitamura and T. Fujiwara, *Acc. Chem. Res.*, 2001, **34**, 633–639.

2 G. Sienel, R. Rieth and K. T. Rowbottom, *Ullmann's Encyclopedia of Industrial Chemistry*, Wiley-VCH Verlag GmbH & Co. KGaA, Weinheim, 2012, vol. 13, DOI: 10.1002/14356007.a09_531.

3 H. D. Swern, *Organic Peroxide*, Wiley Interscience, New York, 1971.
4 (*a*) J. Liu, F. Wang, S. Qi, Z. Gu and G. Wu, *New J. Chem.*, 2013, **37**, 769–774; (*b*) S. Das, A. Goswami, M. HesarI, J. F. Al-Sharab, E. K. Mikmekov, F. Maran and T. Asefa, *Small*, 2014, **10**, 1473–1478; (*c*) S. Anandhakumar, M. Sasidharan, C. W. Tsao and A. M. Raichur, *ACS Appl. Mater. Interfaces*, 2014, **6**, 3275–3281.
5 (*a*) W. Lueangchaichaweng, N. R. Brooks, S. Fiorilli, E. Gobechiya, K. Lin, L. Li, S. Parres-Esclapez, E. Javon, S. Bals, G. V. Tendeloo, J. A. Martens, C. E. A. Kirschhock, P. A. Jacobs and P. P. Pescarmona, *Angew. Chem.*, 2014, **53**, 1585–1589; (*b*) A. Rezaeifard, R. Haddad, M. Jafarpour and M. Hakimi, *ACS Sustainable Chem. Eng.*, 2014, **2**, 942–950.
6 (*a*) M. J. Rak, M. Lerro and A. Moores, *Chem. Commun.*, 2014, **50**, 12482–12485; (*b*) X. Liu, A. Klust, R. J. Madix and C. M. Friend, *J. Phys. Chem. C*, 2007, **111**, 3675–3679; (*c*) A. Dhakshinamoorthy, A. Primo, P. Concepcion, M. Alvaro and H. Garcia, *Chem.–Eur. J.*, 2013, **19**, 7547–7554.
7 S. Sharma, S. Sinha and S. Chand, *Ind. Eng. Chem. Res.*, 2012, **51**, 8806–8814.
8 (*a*) S. S. Acharyya, S. Ghosh, R. Tiwari, C. Pendem, T. Sasaki and R. Bal, *ACS Catal.*, 2015, **5**, 2850–2858; (*b*) S. Ghosh, S. S. Acharyya, R. Tiwari, B. Sarkar, R. K. Singha, C. Pendem, T. Sasaki and R. Bal, *ACS Catal.*, 2014, **4**, 2169–2174; (*c*) M. Stratakis and H. Garcia, *Chem. Rev.*, 2012, **112**, 4469–4506.
9 (*a*) T. Punniyamurthy, S. Velusamy and J. Iqbal, *Chem. Rev.*, 2005, **105**, 2329–2363; (*b*) Y. Nishiyama and Y. N. M. Nakagawa, *Angew. Chem.*, 2001, **40**, 3639–3641; (*c*) J. M. Thomas, R. Raja, G. Sanker and G. Bell, *Nature*, 1999, **398**, 227–230; (*d*) R. Finke and G. H. Weiner, *J. Am. Chem. Soc.*, 1999, **121**, 9831–9842; (*e*) B. Wallar and J. J. D. Lipscomb, *Chem. Rev.*, 1996, **96**, 2625–2658.
10 A. Rezaeifard, R. Haddad, M. Jafarpour and M. Hakimi, *J. Am. Chem. Soc.*, 2013, **135**, 10036–10039.
11 L. Wang, B. Zhang, W. Zhang, J. Zhang, X. Gao, X. Meng, D. S. Su and F. S. Xiao, *Chem. Commun.*, 2013, **49**, 3449–3451.
12 W. Jia, Y. Liu, P. Hu, R. Yu, Y. Wang, L. Ma, D. Wang and Y. Li, *Chem. Commun.*, 2015, **51**, 8817–8820.
13 (*a*) P. Dixneuf and V. Cadierno, *Metal-Catalyzed Reactions in Water*, VCH, New York, 2013; (*b*) U. M. Lindstrom, *Organic Reactions in Water: Principles, Strategies and Applications*, VCH, Weinheim, Germany, 2007.
14 (*a*) M. C. Pirrung and K. D. Sarma, *J. Am. Chem. Soc.*, 2004, **126**, 444–445; (*b*) S. Narayan, J. Muldoon, M. G. Finn, V. V. Fokin, H. C. Kolb and K. B. Sharpless, *Angew. Chem.*, 2005, **117**, 3339–3343; (*c*) B. K. Price and J. M. Tour, *J. Am. Chem. Soc.*, 2006, **128**, 12899–12904.
15 (*a*) X. Liu, A. Klust, R. J. Madix and C. M. Friend, *J. Phys. Chem. C*, 2007, **111**, 3675–3679; (*b*) J. G. Serafin, A. C. Liu and S. R. Seyedmonir, *J. Mol. Catal. A: Chem.*, 1998, **131**, 157–168.
16 (*a*) F. Zaera, *ChemSusChem*, 2013, **6**, 1797–1820; (*b*) Y. Li, Q. Liu and W. Shen, *Dalton Trans.*, 2011, **40**, 5811–5826; (*c*) V. V. Pushkarev, N. Musselwhite, K. An, S. Alayoglu and G. A. Somorjai, *Nano Lett.*, 2012, **12**, 5196–5201.
17 (*a*) J. D. Holmes, K. P. Johnston, R. C. Doty and B. A. Korgel, *Science*, 2000, **287**, 1471–1473; (*b*) B. Goris, S. Bals, W. van den Broek, E. Carbó-Argibay, S. Gómez-Graña, L. M. Liz-Marzán and G. van Tendelo, *Nat. Mater.*, 2012, **11**, 930–935.
18 (*a*) C. Jiang, S. Liu, X. Chen and S. Yu, *CrystEngComm*, 2014, **16**, 8646–8651; (*b*) X. D. Wang, J. H. Song, J. Liu and J. L. Wang, *Science*, 2007, **316**, 102–105.
19 Y. Dai, S. Tang, S. Vongehr and X. Meng, *ACS Sustainable Chem. Eng.*, 2014, **2**, 692–698.
20 R. Xu, X. Wang, D. S. Wang, K. B. Zhou and Y. Li, *J. Catal.*, 2006, **237**, 426–430.
21 Y. Liu, X. Li, C. Shi, J. Liu, A. Zhu and B. W. L. Jang, *Catal. Sci. Technol.*, 2014, **4**, 2589–2598.
22 Z. Qu, Y. Bu, Y. Qin, Y. Wang and Q. Fu, *Appl. Catal., B*, 2013, **132**, 353–362.
23 J. Mao, G. Zhao, D. Wang and Y. A. Li, *RSC Adv.*, 2014, **4**, 25384–25388.
24 (*a*) S. Ghosh, S. S. Acharyya, R. Singh, P. Gupta and R. Bal, *Catal. Commun.*, 2015, **72**, 33–37; (*b*) S. Ghosh, S. S. Acharyya, M. Kumar and R. Bal, *RSC Adv.*, 2015, **5**, 37610–37616; (*c*) S. Ghosh, S. S. Acharyya, S. Adak, L. N. S. Konathala, T. Sasaki and R. Bal, *Green Chem.*, 2014, **16**, 2826–2834; (*d*) S. Ghosh, S. S. Acharyya and R. Bal, *J. Mater. Chem. A*, 2014, **2**, 15726–15733; (*e*) B. Sarkar, R. K. Singha, R. Tiwari, S. Ghosh, S. S. Acharyya, C. Pendem, L. N. S. Konathala and R. Bal, *RSC Adv.*, 2014, **4**, 5453–5456.
25 S. S. Acharyya, S. Ghosh, N. Siddiqui, L. N. S. Konathala and R. Bal, *RSC Adv.*, 2015, **5**, 4838–4843.
26 Y. Lei, F. Mehmood, S. Lee, J. Greeley, B. Lee, S. Seifert, R. E. Winans, J. W. Elam, R. J. Meyer, P. C. Redfern, D. Teschner, R. Schlögl, M. J. Pellin, L. A. Curtiss and S. Vajda, *Science*, 2010, **328**, 224–228.
27 (*a*) J. W. Lee, A. S. Hall, J.-D. Kim and T. E. Mallouk, *Chem. Mater.*, 2012, **24**, 1158–1164; (*b*) D. Wang, Y. Li, Q. Wang and T. Wang, *Eur. J. Inorg. Chem.*, 2012, 628–635.
28 F. Han, F. Chen, Z. Zhong, K. Ramesh, L. Chen and E. Widjaja, *J. Phys. Chem. B*, 2006, **110**, 24450–24456.
29 H. Wang, L.-F. Cui, Y. Yang, H. S. Casalongue, J. T. Robinson, Y. Liang, Y. Cui and H. Dai, *J. Am. Chem. Soc.*, 2010, **132**, 13978–13980.
30 S. S. Acharyya, S. Ghosh and R. Bal, *ACS Appl. Mater. Interfaces*, 2014, **6**, 14451–14459.
31 J. Mondal, P. Borah, S. Sreejith, K. T. Nguyen, X. Han, X. Ma and Y. Zhao, *ChemCatChem*, 2014, **6**, 3518–3529.
32 W. Chen, R. B. Rakhi, Q. Wang, M. N. Hedhili and H. N. Alshareef, *Adv. Funct. Mater.*, 2014, **24**, 3130–3143.
33 Z. Jiang, J. Xie, D. Jiang, X. Wei and M. Chen, *CrystEngComm*, 2013, **15**, 560–569.